Indian Journal of Chemistry
Vol. 63, December 2024, pp. 1250-1262
DOI: 10.56042/ijc.v63i12.14051

Quantum chemical analysis of 3,5-dimethyl-2,6-diphenylpyridine and its *para* amino and nitro phenyl derivatives using density functional theory

Anan Haj Ichia Arisha[a,b]

[a] Department of Organic Chemistry, School of Chemistry, Faculty of Exact Sciences, Tel Aviv University, Tel Aviv 6997801, Israel

[b] Department of Education, Beit Berl College, Beit Berl, Israel

E-mail: ananarisha@gmail.com

Received 29 September 2024; accepted (revised) 27 November 2024

In this study, density functional theory calculations at the wB97XD/Def2TZVPP level have been performed for 3,5-dimethyl-2,6-diphenylpyridine(**1**) compound and its *para* amino phenyl (**2**), *para* nitro phenyl(**3**), *para* amino nitro phenyl (**4**) derivatives. Global reactivity descriptors, namely, ionization potential, electron affinity, electronegativity, chemical potential, chemical hardness, softness, and electrophilicity index have been calculated using the highest occupied molecular orbital (HOMO) and lowest unoccupied molecular orbital (LUMO) energies. In addition, molecular electrostatic potential surfaces, Mulliken and natural charges, natural bond orbitals have been analyzed. Furthermore, ultraviolet–visible (UV–Vis) absorption characteristics and nonlinear optical parameters, *viz*. dipole moment, polarizability, and hyperpolarizability, have been calculated. The range of the energy-gap values (E_{LUMO}− E_{HOMO}) is 6.9470–8.8026 eV, indicating the chemical stability of **1**–**4**, with **4** exhibiting the smallest energy gap, lowest hardness, and most softness. According to the UV–Vis analysis, $\pi\rightarrow\pi^*$ transitions dominate, and in the HOMO–LUMO transition, the wavelength increases in the order of **4**>**3**>**2**>**1**. The hyperpolarizability values change drastically, with the $\beta_{total}/\beta_{urea}$ ratio for **1**, **2**, **3**, and **4** being 2.7, 28, 25, and 50, respectively. These materials, especially **4**, are promising for optoelectronics and industrial applications.

Keywords: 3,5-Dimethyl-2,6-diphenyl, Density functional theory, Natural bond orbital, Ultraviolet–visible, Nonlinear optical parameters

Heterocyclic compounds have garnered significant interest in recent years due to their wide-ranging applications in material science, particularly as fluorescent sensors and electro-luminescent devices[1-5]. Among nitrogen-containing heterocycles, pyridine derivatives stand out for their unique photophysical properties. These compounds find diverse uses as chemosensors, bioprobes, and in light-emitting diodes. A notable contribution to this field comes from Biswal *et al.*[6], who developed a straightforward and efficient method for synthesizing 3,5-dimethyl-2,6-diphenylpyridine(**1**) and other pyridines using 1,5-diketones as precursors and cobalt (II) porphyrin (Co-por) as a catalyst, as illustrated in Scheme 1.

Adding substituents such as amino or nitro groups (for instance, compounds **2**–**4**) to the structure of compound 1 may enhance the electronic and photophysical characteristics of these substances. The development of organic materials with effective nonlinear optical (NLO) properties is increasingly significant due to their potential in advanced optoelectronic applications[7-9]. Numerous computational studies have explored the relationship between molecular structure and electronic properties[10-16], leading to materials suitable for advanced technology and industry.

In this study, we computationally examined the amino and nitro derivatives of pyridine **1**. The amino donating and nitro withdrawing effects may alter the electronic properties of compounds **2**–**4**, facilitating the development of novel compounds for modern technology applications. Density functional theory (DFT) calculations were conducted at the wB97XD/Def2TZVPP level to optimize the structures of compounds **1**–**4**. Global reactivity descriptors, including ionization potential (IP), electron affinity (EA), electronegativity (χ), chemical potential (μ), chemical hardness (η), softness (σ), electrophilicity index (ω), were determined from the energy values of the highest occupiedmolecular orbital (HOMO) and lowest unoccupied molecular orbital (LUMO). Moreover, molecular electrostatic potential (MEP) surfaces, Mulliken and natural charges, and natural bond orbitals (NBOs) of the titled compounds were analyzed. Additionally, ultraviolet–visible

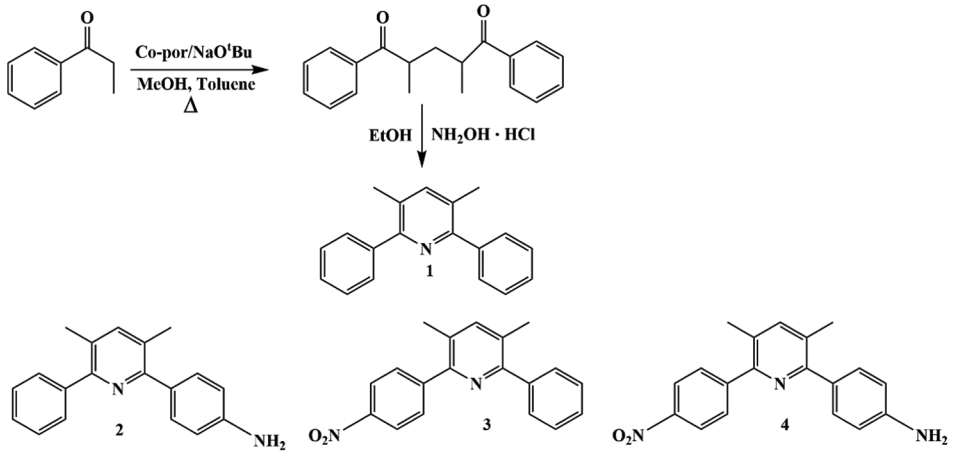

Scheme 1 — Synthetic route for pyridines derivatives

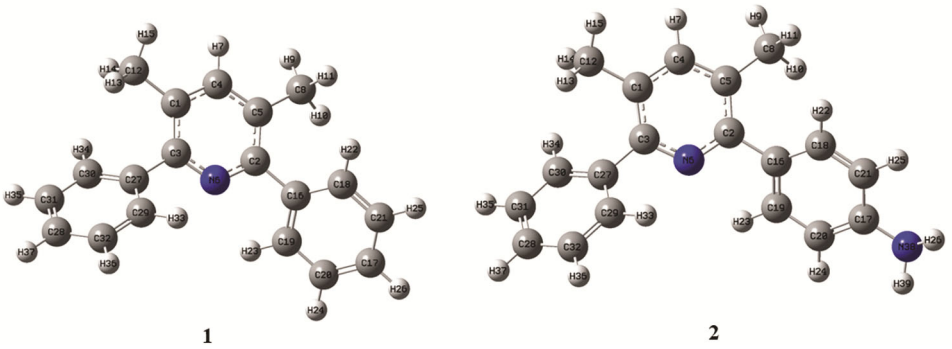

Fig. 1 — Optimized structures of **1** and **2**

(UV–Vis) absorption calculations are performed using time-dependent (TD)-DFT with the Def2TZVPP basis set. Finally, dipole moment, polarizability (α), and hyperpolarizability (β) were utilized to predict the NLO activity of compounds **1**–**4**.

Computational Methods

DFT calculations were performed using the Gaussian 16 software[17] and GaussView 6.0 interface[18]. All the geometric optimizations and frequency calculations were performed using the wB97XD-DFT method, which included empirical dispersion and long-range corrections. The valence and triple zeta Def2TZVPP frameworks were utilized as the basis set with the keyword "opt+freq," and all the stationary points were identified as minima (zero imaginary frequencies). The NBO calculations were performed at the same level of theory with the keyword: pop = (nbo, savenbos). Furthermore, the electronic UV–Vis spectrum was obtained by TD-DFT using wB97XD/Def2TZVPP with the following keywords:td=(nstates=6,root=1) pop=full density=current int=ultrafine iop(9/40=3).

The NLO parameters were calculated at the same level using the word "polar". The values of the total energy with thermal correction (ΔE), enthalpy (ΔH), and Gibbs energy (ΔG) were determined under the standard conditions of 298.15 K and 1 atm in a gas phase. The Cartesian coordinates and thermodynamic parameters of all the calculated structures are provided in the Supplementary Material.

Results and Discussion

Molecular geometry

The initial step involved is geometry optimization to ascertain the structures of compounds **1**,**2**,**3**, and **4**. Fig. 1 and 2 present the optimized geometries of compounds **1**–**4**, with bond lengths, bond angles, and dihedral angles detailed in Table 1. The three rings are optimally arranged. In compound **1**, the benzene ring is twisted away from the methyl group and slightly oriented toward the pyridine nitrogen, with dihedral angles C5C2C16C18 and N6C2C16C19 at 47.0175° and 43.6106°, respectively (Table 1). In compound **2**, the amino benzene group is more

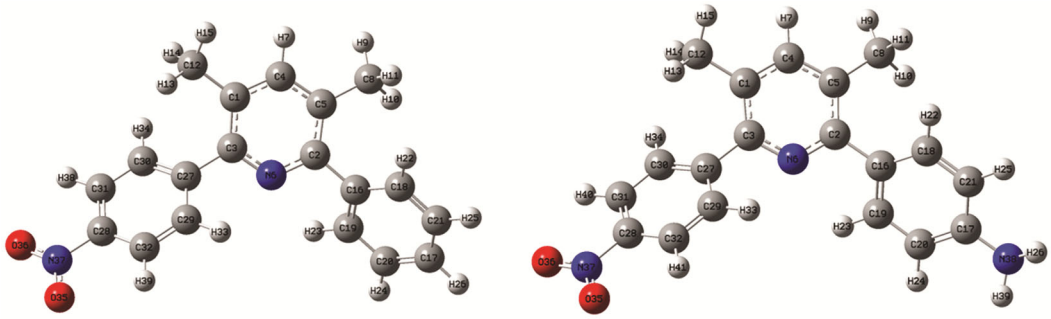

3 **4**

Fig. 2 — Optimized structures of **3** and **4**

Table 1 — Some selected geometric parameters of 1, 2, 3 and 4

Bond lengths (Å)	1	2	3	4
N6–C3	1.3295	1.3296	1.3295	1.3294
N6–C2	1.3295	1.3306	1.3286	1.3299
C3–C27	1.4880	1.4883	1.4880	1.4882
C2–C16	1.4880	1.4845	1.4874	1.4836
N38–C17		1.3890		1.3869
N38–H26		1.0049		1.0047
N37–O35			1.2122	1.2124
N37–C28			1.4711	1.4705
Bond angles (°)				
N6C3C27	114.9578	114.8902	114.4854	114.4079
N6C2C16	114.9578	115.0850	115.0929	115.1803
C3C27C30	121.9622	122.0247	121.9638	121.9952
C2C16C18	121.9622	122.7418	121.8332	122.7233
C3C27C29	119.2909	119.2745	119.0825	119.0784
C2C16C19	119.2909	119.5819	119.3373	119.5687
C17N38H26		115.5591		115.8413
H26N38H39		112.3664		112.6258
C28N37O35			117.6760	117.6834
O35N37O36			124.6575	124.6149
Dihedral angle (°)				
C1C3C27C30	47.0175	46.7913	45.5745	45.7083
C5C2C16C18	47.0175	44.6560	47.7285	44.7510
N6C3C27C29	43.6106	43.2484	42.1017	42.1151
N6C2C16C19	43.6106	40.6146	44.4365	40.7078
C1C3C27C29	–135.0387	–135.2712	–136.5767	–136.4797
C5C2C16C19	–135.0387	–137.8869	–134.3537	–137.8167
N6C2C16C18	–134.3332	–136.8426	–133.4813	–136.7245
N6C3C27C30	–134.3332	–134.6892	–135.7470	–135.6969
C21C17N38H26		24.0148		23.4785
C20C17N38H26		–158.3157		–158.8469
C31C28N37O35			179.7850	179.7554
C32C28N37O35			0.1479	0.1344

aligned with the pyridine nitrogen, with N6C2C16C19 at 40.6146°, indicating strong attraction between the rings. Compound **3** has a dihedral angle N6C3C27C29 of 42.1017°, while compound **4** has N6C2C16C19 at 40.7078° and N6C3C27C29 at 42.1151°, similar to compounds **2** and **3**, respectively. The nitro group in compound **3** is planar with the benzene ring, with a dihedral angle C31C28N37O35 at 179.7850°. The amino group in compound **2** deviates slightly from the benzene ring plane, with a dihedral angle C21C17N38H26 at 24.0148°. The N6–C2 bond length in compound

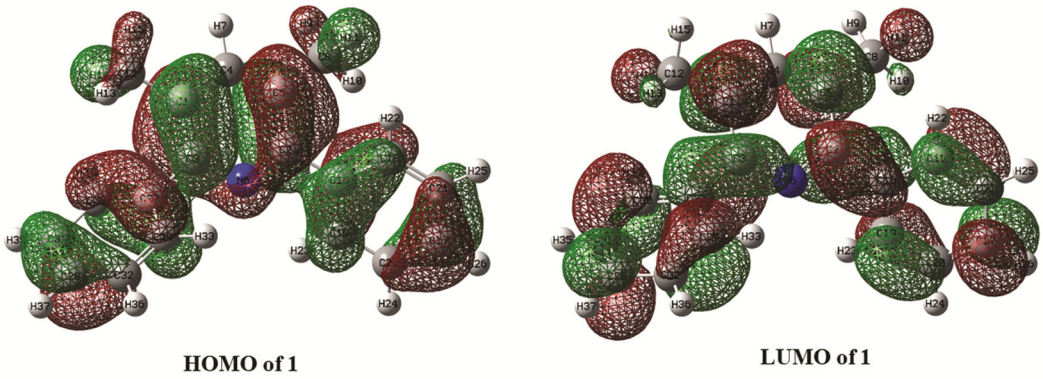

Fig. 3 — HOMO and LUMO of **1**

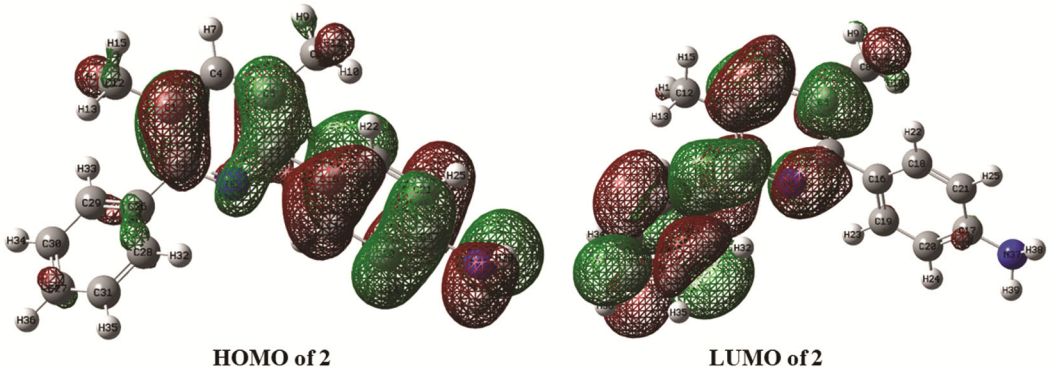

Fig. 4 — HOMO and LUMO of **2**

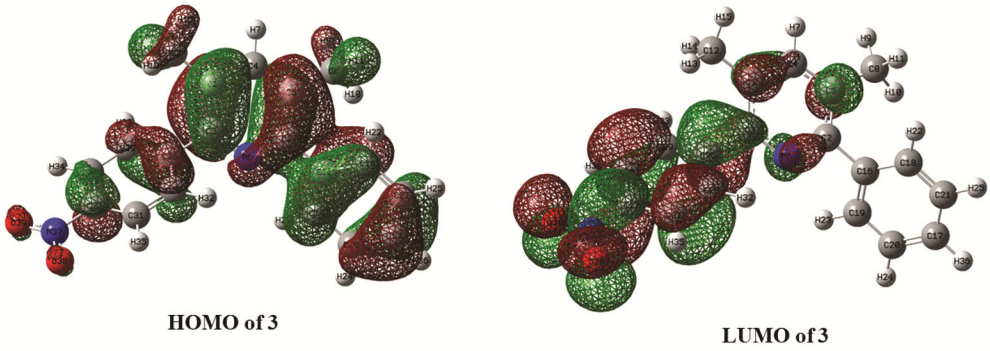

Fig. 5 — HOMO and LUMO of **3**

2 (1.3306Å) is slightly longer than that in compound **1** (1.3295Å), and the C2–C16 bond length in **2** (1.4845 Å) is shorter than that in **1** (1.4880Å), suggesting resonance donation from the amino benzene ring to the pyridine ring.

Frontier molecular orbital analysis

The HOMOs and the LUMOs are known as frontier molecular orbitals. HOMO energy reflects a molecule's electron-donating ability, while LUMO energy reflects its electron-accepting ability. The energy gap between HOMO and LUMO correlates with a compound's kinetic stability; smaller gaps indicate a greater tendency for polarization and higher chemical reactivity, implying lower kinetic stability. Fig. 3-6 show the HOMO and LUMO orbitals of compounds **1**–**4**, and Table 2 lists the HOMO, LUMO energies, and energy gaps (E_{LUMO}- E_{HOMO}). In compound **1**, the HOMO and LUMO electron densities are distributed around the three rings: pyridine and the two benzene rings.

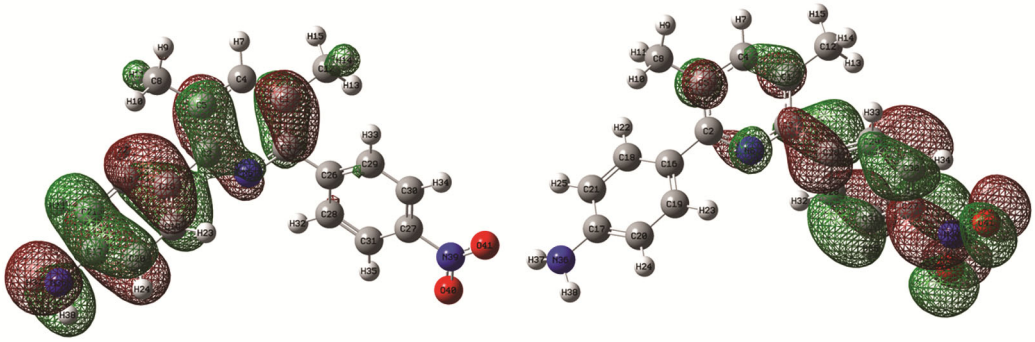

HOMO of 4 LUMO of 4

Fig. 6 — HOMO and LUMO of **4**

Table 2 — Global reactivity parameters of 1–4 (all values in eV and σ is in $(eV)^{-1}$)

Parameters	1	2	3	4
E_{HOMO}	–8.0581	–7.3669	–8.4481	–7.5933
E_{LUMO}	0.7445	0.8825	–0.7127	–0.6463
$\Delta E= E_{LUMO}- E_{HOMO}$	8.8026	8.2494	7.7354	6.9470
IP	8.0581	7.3669	8.4481	7.5933
EA	–0.7445	–0.8825	0.7127	0.6463
χ	3.6568	3.2422	4.5804	4.1198
μ	–3.6568	–3.2422	–4.5804	–4.1198
η	4.4013	4.1247	3.8677	3.4735
σ	0.2272	0.2424	0.2586	0.2879
ω	1.5191	1.2743	2.7122	2.4432

Amino group substitution on one benzene ring, as in compound **2**, concentrates the HOMO at the amino benzene and pyridine rings, whereas the LUMO is located at the unsubstituted benzene and pyridine, indicating charge transfer from the amino benzene to the benzene ring *via* the pyridine ring. By contrast, in compound **3**, which contains a withdrawing nitro group on one benzene ring, the LUMO is mainly concentrated around the nitro benzene moiety, while the HOMO is spread around the unsubstituted benzene, pyridine, and slightly toward the nitro benzene. Charge transfer occurs from benzene to nitro benzene *via* the pyridine ring. In compound **4**, charge transfer occurs from the amino benzene to the nitro benzene ring (Fig. 6). The HOMO and LUMO energies of compounds **1–4** were calculated to examine their electronic properties. The amino group's donation increases the HOMO and LUMO energies, whereas the nitro group's withdrawal reduces them (Table 2). Additionally, the energy gaps (E_{LUMO}− E_{HOMO}) ranging from 6.9470 to 8.8026 eV suggest that compounds **1–4** are chemically stable, with compound **4** being the most reactive owing to its smallest energy gap (Table 2).

Global reactivity descriptors

Global descriptive parameters elucidate intramolecular charge transfer and chemical reactivity. Key global reactivity descriptors include IP, EA, electronegativity (χ), chemical potential (μ), chemical hardness (η), softness (σ), electrophilicity index (ω). These are determined using HOMO and LUMO energy values through the following specificequations:

$$IP = -E_{HOMO} \quad \text{... (1)}$$

$$EA = -E_{LUMO} \quad \text{... (2)}$$

$$\chi = \frac{IP+EA}{2} = -\frac{(E_{HOMO}+E_{LUMO})}{2} \quad \text{... (3)}$$

$$\mu = -\chi = \frac{(E_{HOMO}+E_{LUMO})}{2} \quad \text{... (4)}$$

$$\eta = \frac{IP-EA}{2} = \frac{(E_{LUMO}-E_{HOMO})}{2} \quad \text{... (5)}$$

$$\sigma = \frac{1}{\eta} = \frac{2}{(E_{LUMO}-E_{HOMO})} \quad \text{... (6)}$$

$$\omega = \frac{\mu^2}{2\eta} \quad \text{... (7)}$$

IP is the minimum energy needed to remove an electron from the outermost shell of an isolated gaseous particle. EA is the energy change when a gaseous particle gains an electron. Electronegativity (χ) describes a molecule's ability to attract electrons, while chemical potential (μ) indicates the energy change when adding an electronic charge. Chemical hardness (η) reflects resistance to polarization, and softness (σ) indicates the capacity to accept electrons. The electrophilicity index (ω) measures a molecule's electrophilicity, with higher values indicating better electrophiles.

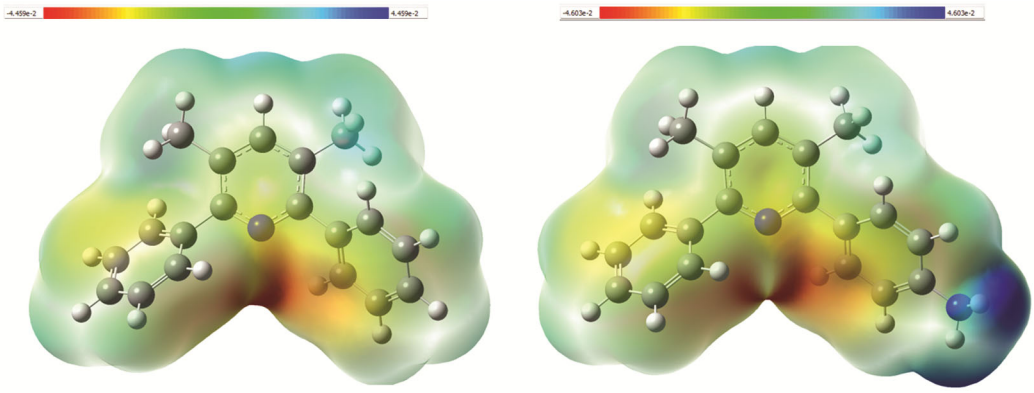

1 2

Fig. 7 — MEPs of compounds **1** and **2**

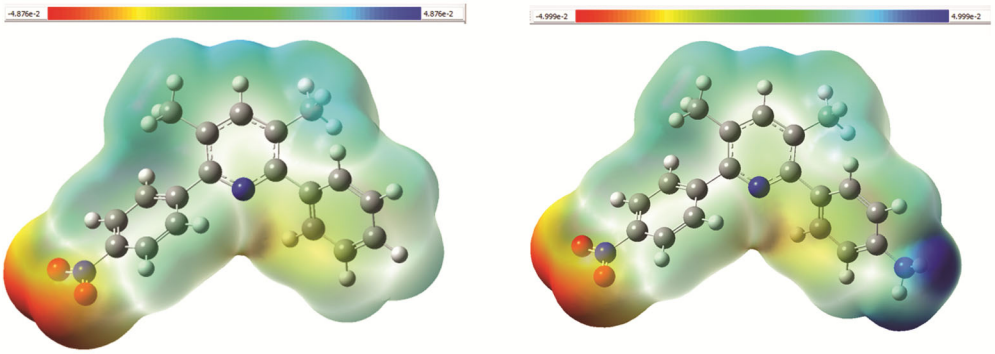

3 4

Fig. 8 — MEPs of compounds **1** and **2**

Table 2 presents the global reactivity parameters of compounds **1**–**4**. Compound **2** exhibits the lowest IP owing to the electron-donating amino group. Compound **3** has the highest EA, electronegativity (χ), and electrophilicity index (ω) because of the electron-withdrawing nitro group. Compound **4** has the lowest hardness and highest softness, and is thus characterized by a highly mobile electron cloud.

MEP

The MEP illustrates electrostatic potential on a constant electron density surface. This potential is color-coded, increasing as follows: red < orange < yellow < green < blue. The red area, rich in electrons, suggests an electrophilic attack site, whereas the blue area, electron-deficient, indicates a nucleophilic attack site. Green represents a neutral area. Fig. 7 and 8 display the MEPs of compounds **1**–**4**.

In compound **1**, the pyridine nitrogen exhibits a negative potential due to nitrogen's withdrawing effect, with the positive potential distributed among the C–H bonds. In compound **2**, the amino group's resonance donating effect causes the positive potential to localize on the amino nitrogen, while the negative potential resides on the pyridine nitrogen. In compound **3**, the negative potential is localized around the electron-withdrawing nitro group. In compound **4**, the positive potential is concentrated on the amino group, while the negative potential is observed on the nitro group.

Population analysis

Mulliken population analysis (MPO) and natural population analysis (NPO) are essential for determining atomic charges, impacting properties like dipole moment, molecular polarizability, and electronic structure. NPO offers a better description of electronic charge distribution than MPO. Atomic charges are numerically calculated or visually represented by a color gradient from red (most negatively charged) to green (most positively charged). Table 3 presents the Mulliken and NBO

Table 3 — Mulliken and NBO chargesof compound 1–4

Atom number	Mulliken charges				NBO charges			
	1	2	3	4	1	2	3	4
C1	–0.0272	–0.0292	–0.0325	–0.0331	–0.0412	–0.0467	–0.0365	–0.0422
C2	0.3089	0.2764	0.3129	0.2822	0.1844	0.1948	0.1885	0.1990
C3	0.3089	0.3118	0.2909	0.2945	0.1844	0.1834	0.1679	0.1669
C4	–0.0961	–0.0955	–0.0897	–0.0873	–0.1583	–0.1581	–0.1572	–0.1571
C5	–0.0272	–0.0236	–0.0245	–0.0195	–0.0412	–0.0455	–0.0332	–0.0375
N6	–0.3222	–0.3239	–0.3261	–0.3313	–0.4094	–0.4145	–0.4068	–0.4123
H7	0.0879	0.0861	0.0913	0.0901	0.2026	0.2013	0.2053	0.2040
C8	–0.2573	–0.2648	–0.2521	–0.2669	–0.6263	–0.6257	–0.6278	–0.6271
H9	0.0872	0.0858	0.0885	0.0880	0.2149	0.2137	0.2165	0.2152
H10	0.1101	0.1118	0.1116	0.1140	0.2303	0.2303	0.2320	0.2320
H11	0.0954	0.0942	0.0972	0.0966	0.2165	0.2144	0.2190	0.2168
C12	–0.2573	–0.2583	–0.2593	–0.2671	–0.6263	–0.6255	–0.6279	–0.6270
H13	0.1101	0.1094	0.1112	0.1099	0.2303	0.2293	0.2286	0.2275
H14	0.0954	0.0944	0.0983	0.0985	0.2165	0.2152	0.2182	0.2170
H15	0.0872	0.0863	0.0903	0.0909	0.2149	0.2142	0.2191	0.2183
C16	0.0143	0.0013	0.0060	–0.0065	–0.0643	–0.1177	–0.0685	–0.1231
C17	–0.1061	0.1880	–0.1035	0.1865	–0.2087	0.1679	–0.2057	0.1712
C18	–0.2205	–0.2098	–0.2178	–0.2116	–0.1974	–0.1649	–0.1964	–0.1635
C19	–0.1657	–0.1585	–0.1656	–0.1623	–0.1766	–0.1452	–0.1766	–0.1446
C20	–0.1280	–0.1640	–0.1288	–0.1597	–0.2082	–0.2655	–0.2068	–0.2650
C21	–0.1285	–0.1623	–0.1286	–0.1596	–0.2108	–0.2705	–0.2093	–0.2699
H22	0.1217	0.1194	0.1218	0.1223	0.2085	0.2092	0.2089	0.2095
H23	0.1088	0.1053	0.1083	0.1058	0.2265	0.2266	0.2254	0.2256
H24	0.1173	0.0941	0.1195	0.0961	0.2122	0.2064	0.2138	0.2078
H25	0.1163	0.0920	0.1184	0.0935	0.2113	0.2054	0.2128	0.2067
H26	0.1184	0.1237	0.1206	0.1263	0.2114	0.3746	0.2130	0.3762
C27	0.0143	0.0108	0.0277	0.0283	–0.0643	–0.0623	–0.0243	–0.0216
C28	–0.1061	–0.1068	–0.0306	–0.0337	–0.2087	–0.2100	0.0165	0.0151
C29	–0.1657	–0.1667	–0.1383	–0.1434	–0.1766	–0.1771	–0.1755	–0.1763
C30	–0.2205	–0.2195	–0.2034	–0.2076	–0.1974	–0.1977	–0.1970	–0.1975
C31	–0.1285	–0.1292	–0.0826	–0.0813	–0.2108	–0.2113	–0.1858	–0.1858
C32	–0.1280	–0.1283	–0.0981	–0.0946	–0.2082	–0.2090	–0.1843	–0.1848
H33	0.1088	0.1081	0.1171	0.1177	0.2265	0.2266	0.2364	0.2364
H34	0.1217	0.1209	0.1308	0.1327	0.2085	0.2085	0.2178	0.2178
H35	0.1163	0.1156			0.2113	0.2108		
H36	0.1173	0.1161			0.2122	0.2114		
H37	0.1184	0.1176			0.2114	0.2108		
N38		–0.2534		–0.2505		–0.7831		–0.7813
H38			0.1504				0.2485	
H39		0.1246	0.1507	0.1276		0.3753	0.2490	0.3769
N37			0.4959	0.4951			0.5232	0.5234
O35			–0.3380	–0.3397			–0.3690	–0.3703
O36			–0.3400	–0.3413			–0.3717	–0.3724
H40				0.1501				0.2480
H41				0.1505				0.2483

charges of compounds **1**–**4**, while Fig. 9 illustrates the dipole moments and NBO charge distribution of these compounds.

Table 3 and Fig. 9 show that hydrogen atoms are positively charged due to their lower electronegativity compared to carbon. The pyridine nitrogen, being an electron withdrawer, is negatively charged, making the bonded carbon positive. Methyl carbons exhibit negative charges, influenced by the positivity of adjacent carbons. For compounds **2** and **4**, the amino

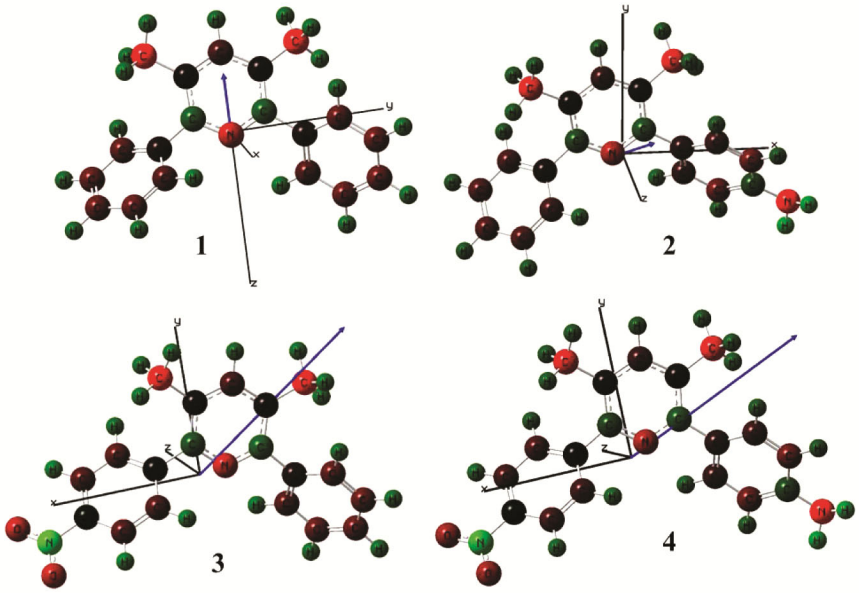

Fig. 9 — Moment dipoles and NBO charge distributions of compounds **1–4**

nitrogen carries a negative charge owing to its electronegativity. In compounds **3** and **4**, nitro nitrogen is positively charged, with the electron-withdrawing oxygens being negative.

NBO analysis

NBO analysis is a robust tool for elucidating the overall charge distribution in a molecule and the transfer of electrons from donor to acceptor. It quantifies delocalization or hyperconjugation interactions, intramolecular hydrogen bonding, intramolecular charge transfer, and bond interactions. Utilizing the second-order Fock matrix, the stabilization energies of various donor–acceptor interactions on the NBO basis were calculated as:

$$E(2) = \Delta E_{i,j} = -q_i \frac{F^2(i,j)}{\varepsilon_i - \varepsilon_j} \quad \text{... (8)}$$

where $E(2)$ is the stabilization energy, q_i is the donor orbital occupancy, ε_i and ε_j are diagonal elements, and F(i,j) is the Fock matrix element. A strong interaction between *i* and *j* occurs when $E(2)$ is increased, resulting in significant conjugation throughout the system. Table 4 and Table 5 present the Fock matrix analysis in the NBO basis for **1–4** performed using the second-order perturbation theory. NBO analysis reveals donor–acceptor interactions within each aromatic ring.

In compound **1**, for example, the donors π(C1–C3) (HOMO-2), π(C4–C5) (HOMO-7), and π(C16–C18) (HOMO-4) interact with the LUMO acceptor π*(C2–N6), and the HOMO donor π(C29–C32) interacts with π*(C27–C30) (LUMO+5). Strong interactions occur between the LUMO donor π*(C2–N6) and the acceptors π*(C1–C3) (LUMO+4), π*(C4–C5) (LUMO+3), and π*(C16–C18) (LUMO+6), as shown in Table 4. In addition, the amino group stimulates other interaction; for example, in **2,** the LUMO+1 donor π*(C17–C21) strongly interacts with the acceptors π*(C16–C18) (LUMO+6) and π*(C19–C20) (LUMO+8). Moreover, the lone pairs (LP) of the amino nitrogen (HOMO-9) are donated to the π*(C17–C21) bond. In compounds **3** and **4**, enhanced interactions occur within the nitro group as well as between the benzene's double bond and the nitro group's N–O bond. Specifically, in compound **4**, the donor region (C28–C31) (HOMO-8) interacts with the LUMO (N37–O35) bond.

UV–Vis spectrum analysis

UV–Vis spectroscopy is essential for material analysis and structural determination. The time-dependent self-consistent field (TD-DFT) method calculates the maximum absorption wavelength (λ_{max}), oscillator strength (*f*), and corresponding electron orbital transitions. An increase in oscillator strength indicates a higher probability of electronic transitions. Table 6 presents the electronic absorbance parameters for compounds **1–4**. The dominant absorptions for these compounds are HOMO–LUMO and HOMO–LUMO+1 transitions, which are $\pi \rightarrow \pi^*$ transitions. For

Table 4 — Results of the analysis of the Fock matrix in the NBO basis for compounds **1** and **2** using the second-order perturbation theory

Donor NBO (i)	Acceptor NBO (j)	E(2) kcal/mol		E(j)-E(i) a.u.		F(i,j) a.u.	
		1	2	1	2	1	2
π(C1–C3)	π*(C2–N6)	34.52	33.57	0.36	0.36	0.100	0.099
π(C1–C3)	π*(C4–C5)	38.11	38.23	0.38	0.38	0.110	0.110
π(C2–N6)	π*(C1–C3)	39.02	39.71	0.44	0.44	0.119	0.120
π(C2–N6)	π*(C4–C5)	22.12	21.94	0.44	0.44	0.089	0.088
π(C4–C5)	π*(C1–C3)	31.49	31.16	0.40	0.40	0.100	0.099
π(C4–C5)	π*(C2–N6)	44.52	43.79	0.37	0.37	0.116	0.116
π(C16–C18)	π*(C2–N6)	10.50	12.81	0.36	0.36	0.056	0.062
π(C16–C18)	π*(C17–C21)	35.17	28.45	0.38	0.37	0.104	0.093
π(C16–C18)	π*(C19–C20)	32.79	38.23	0.39	0.39	0.102	0.109
π(C17–C21)	π*(C16–C18)	34.29	42.37	0.39	0.39	0.104	0.115
π(C17–C21)	π*(C19–C20)	33.07	26.94	0.39	0.39	0.102	0.093
π(C19–C20)	π*(C16–C18)	35.28	27.06	0.39	0.39	0.105	0.094
π(C19–C20)	π*(C17–C21)	36.09	36.58	0.38	0.38	0.105	0.108
π(C27–C30)	π*(C28–C31)	35.17	35.38	0.38	0.38	0.104	0.104
π(C27–C30)	π*(C29–C32)	32.79	32.85	0.39	0.39	0.102	0.102
π(C28–C31)	π* (C27–C30)	34.29	34.06	0.39	0.39	0.104	0.104
π(C28–C31)	π*(C29–C32)	33.07	33.07	0.39	0.39	0.102	0.102
π(C29–C32)	π* (C27–C30)	35.28	35.16	0.39	0.39	0.105	0.105
π(C29–C32)	π*(C28–C31)	36.09	36.11	0.38	0.38	0.105	0.105
LP (N6)	σ*(C1–C3)	14.46	14.51	1.02	1.02	0.110	0.110
LP (N6)	σ*(C2–C5)	14.45	14.34	1.02	1.02	0.110	0.109
π*(C2–N6)	π*(C1–C3)	187.84	198.27	0.02	0.02	0.099	0.099
π*(C2–N6)	π*(C4–C5)	236.76	242.31	0.02	0.02	0.104	0.103
π*(C2–N6)	π*(C16–C18)	57.14	69.65	0.03	0.02	0.055	0.058
π*(C17–C21)	π*(C16–C18)		299.38		0.02		0.098
π*(C17–C21)	π*(C19–C20)		237.02		0.02		0.092
LP (N38)	π*(C17–C21)		36.63		0.45		0.122

Table 5 — Results of the analysis of the Fock matrix in the NBO basis for compounds **3** and **4** using the second-order perturbation theory

Donor NBO (i)	Acceptor NBO (j)	E(2) kcal/mol		E(j)-E(i) a.u.		F(i,j) a.u.	
		3	4	3	4	3	4
π(C1–C4)	π*(C3–N6)	45.43	45.86	0.37	0.37	0.117	0.177
π(C1–C4)	π*(C2–C5)	31.68	31.30	0.40	0.40	0.100	0.100
π(C3–N6)	π*(C1–C4)	22.13	21.78	0.44	0.44	0.089	0.089
π(C3–N6)	π*(C2–C5)	38.15	37.79	0.45	0.45	0.118	0.118
π(C2–C5)	π*(C1–C4)	38.23	39.28	0.38	0.38	0.110	0.111
π(C2–C5)	π*(C3–N6)	36.26	36.31	0.36	0.35	0.102	0.101
π(C16–C18)	π*(C2–C5)	9.54	11.79	0.39	0.38	0.054	0.06
π(C16–C18)	π*(C17–C21)	34.69	28.03	0.39	0.37	0.104	0.093
π(C16–C18)	π*(C19–C20)	32.76	38.15	0.39	0.39	0.102	0.109
π(C17–C21)	π*(C16–C18)	34.78	43.18	0.39	0.39	0.105	0.116
π(C17–C21)	π*(C19–C20)	33.19	26.84	0.39	0.39	0.103	0.093
π(C19–C20)	π*(C16–C18)	35.47	26.96	0.39	0.39	0.105	0.094
π(C19–C20)	π*(C17–C21)	35.92	36.38	0.38	0.38	0.105	0.108
π(C27–C30)	π*(C3–N6)	10.15	9.99	0.37	0.37	0.055	0.055
π(C27–C30)	π*(C28–C31)	41.37	41.71	0.37	0.37	0.111	0.111
π(C27–C30)	π*(C29–C32)	29.34	29.34	0.39	0.39	0.098	0.098
π(C28–C31)	π* (C27–C30)	28.98	28.75	0.41	0.41	0.097	0.097

(*contd.*)

Table 5 — Results of the analysis of the Fock matrix in the NBO basis for compounds **3** and **4** using the second-order perturbation theory (*contd.*)

Donor NBO (i)	Acceptor NBO (j)	E(2) kcal/mol		E(j)-E(i) a.u.		F(i,j) a.u.	
π(C28–C31)	π*(C29–C32)	32.12	32.09	0.41	0.41	0.104	0.104
π(C29–C32)	π* (C27–C30)	37.17	37.05	0.39	0.39	0.108	0.108
π(C29–C32)	π*(C28–C31)	35.89	35.80	0.37	0.37	0.104	0.104
LP (N6)	σ*(C1–C3)	14.50	14.56	1.02	1.02	0.110	0.110
LP (N6)	σ*(C2–C5)	14.35	14.21	1.02	1.02	0.109	0.109
π*(C3–N6)	π*(C1–C4)	206.37	216.93	0.02	0.02	0.105	0.105
π*(C3–N6)	π*(C2–C5)	159.87	157.24	0.03	0.03	0.099	0.099
π*(C3–N6)	π*(C27–C30)	76.79	84.05	0.02	0.02	0.057	0.057
π*(C28–C31)	π*(C27–C30)	258.15	243.08	0.02	0.02	0.100	0.100
π*(C28–C31)	π*(C29–C32)	183.28	180.48	0.02	0.02	0.096	0.096
π(C28–C31)	π*(N37–O35)	30.27	30.54	0.24	0.24	0.081	0.081
π(N37–O35)	LP(O36)	10.88	10.86	0.23	0.23	0.084	0.084
LP(O35)	π*(N37–C28)	18.80	18.71	0.70	0.70	0.102	0.102
LP(O35)	σ* (N37–O36)	25.60	25.90	0.88	0.88	0.136	0.136
LP(O36)	σ* (N37–O35)	25.52	25.53	0.88	0.88	0.136	0.136
LP(O36)	π*(N37–O35)	251.28	251.10	0.22	0.22	0.212	0.212
LP(O36)	σ*(N37–C28)	18.75	18.68	0.70	0.70	0.102	0.102
π*(N37–O35)	π*(C28–C31)	18.43	18.48	0.15	0.15	0.068	0.068
π*(C17–C21)	π*(C16–C18)		341.46		0.01		0.098
π*(C17–C21)	π*(C19–C20)		241.42		0.02		0.092
LP (N38)	π*(C17–C21)		37.80		0.44		0.124

Table 6 — Electronic absorbance parameters for compounds **1–4.** (H: HOMO; L: LOMO)

Excited state	Excitation energies *E*(eV)	Wavelength λ(nm)	Oscillator strength (*f*)	Assignments		
			Compound 1			
1	4.8430	256.01	0.2066	H–(L+1) (63%)	(H-4)–(L+1) (12%)	(H-2)–(L+1) (9%)
2	4.9670	249.61	0.1002	(H-4)–(L+1) (41%)	(H-2)–(L+1) (28%)	H–(L+1) (20%)
3	5.1360	241.40	0.1331	H–L (44%)	(H-2)–L (22%)	(H-4)–L (17%)
4	5.2992	233.97	0.1296	H–L (36%)	(H-2)–L (29%)	(H-1)–(L+3) (6%)
5	5.3372	232.30	0.0010	(H-3)–L (24%)	H–(L+3) (20%)	(H-1)–(L+2) (19%)
6	5.3706	230.86	0.0237	H–(L+2) (15%)	(H-1)–(L+3) (11%)	(H-3)–(L+1) (9%)
			Compound 2			
1	4.7037	263.59	0.4162	H–(L+1) (55%)	H–L (16%)	(H-1)–(L+1) (7%)
2	4.8462	255.84	0.0114	H–(L+3) (40%)	H–(L+2) (35%)	(H-2)–(L+1) (5%)
3	4.9312	251.43	0.1417	(H-2)–L (21%)	(H-4)–L (17%)	H–(L+1) (16%)
4	4.9952	248.21	0.2001	H–L (33%)	H–(L+1) (15%)	(H-4)–(L+1) (12%)
5	5.2580	235.80	0.0288	(H-2)–L (27%)	(H-2)– (L+1) (18%)	(H-4)–(L+1) (17%)
6	5.3540	231.57	0.0059	(H-4)–L (26%)	(H-3)–L (15%)	(H-1)–(L+2) (14%)
			Compound 3			
1	4.0686	304.73	0.0005	(H-7)–L (79%)	(H-7)– (L+2) (12%)	(H-7)– (L+5) (3%)
2	4.5540	272.25	0.0019	(H-8)–L (81%)	(H-8)– (L+2) (11%)	(H-8)– (L+5) (3%)
3	4.5903	270.10	0.5129	H–L (54%)	(H-2)–L (17%)	H–(L+2) (9%)

(*contd.*)

Table 6 — Electronic absorbance parameters for compounds **1–4.** (H: HOMO; L: LOMO) (*contd.*)

Excited state	Excitation energies *E*(eV)	Wavelength λ(nm)	Oscillator strength (*f*)	Assignments		
4	4.8054	258.01	0.0587	(H-3)–L (41%)	(H-4)–L (17%)	(H-3)– (L+2) (10%)
5	4.9017	252.94	0.0150	(H-4)–L (46%)	(H-3)– (L+1) (14%)	(H-3)– (L+2) (12%)
6	4.9975	248.09	0.1343	H–(L+1) (57%)	(H-2)–L (10%)	(H-4)–L (4%)
			Compound 4			
1	4.0698	304.64	0.0008	(H-7)–L (81%)	(H-7)– (L+2) (11%)	(H-7)– (L+5) (4%)
2	4.4327	279.70	0.3907	H–L (41%)	(H-1)–L (27%)	H–(L+1) (11%)
3	4.5581	272.01	0.0016	(H-8)–L (83%)	(H-8)– (L+2) (11%)	(H-8)– (L+5) (3%)
4	4.7674	260.06	0.3769	H–(L+1) (59%)	(H-3)–L (7%)	H–(L+5) (4%)
5	4.7818	259.28	0.0283	(H-3)–L (31%)	(H-4)–L (15%)	(H-3)– (L+2) (9%)
6	4.8525	255.50	0.0718	H–(L+4) (68%)	(H-2)– (L+1) (8%)	H–(L+1) (6%)

the HOMO–LUMO transition, the absorption wavelength increases in the order **4**>**3**>**2**>**1**, corresponding to the decreasing HOMO–LUMO energy gaps. A smaller energy gap results in longer wavelength absorption owing to the amino and nitro conjugation effect.

NLO properties

Nonlinear optical (NLO) materials exhibit significant applicability in optoelectronics, telecommunications, digital data writing, and the laser industry. NLO properties can be characterized by the following parameters: dipole moment (μ), molecular polarizability (α), and hyperpolarizability (β). μ serves as a measure of the net polarity of materials, while α describes the molecule's distortion in the presence of an electric field. μ_{total} and the mean polarizability <α> are defined as follows:

$$\mu_{total} = \left(\mu_x^2 + \mu_y^2 + \mu_z^2\right)^{1/2} \quad \ldots (9)$$

$$< \alpha >= 1/3\left(\alpha_{xx} + \alpha_{yy} + \alpha_{zz}\right) \quad \ldots (10)$$

where, α_{xx}, α_{yy}, and $\alpha_{zz}$are the principal values of the polarizability tensor. β_{total} (first-order hyperpolarizability) shows the optical nonlinearity activity of materials and can be calculated using the following equations:

$$\beta_{total} = \left[\beta_x{}^2 + \beta_y{}^2 + \beta_z{}^2\right]^{1/2} \quad \ldots (11)$$

where,

$$\beta_x = \beta_{xxx} + \beta_{xyy} + \beta_{xzz}$$

$$\beta_y = \beta_{yyy} + \beta_{xxy} + \beta_{yzz}$$

$$\beta_z = \beta_{zzz} + \beta_{xxz} + \beta_{yyz}.$$

Urea, with a β_{total} of 0.3704×10^{-30} e.s.u. (electrostatic units), is commonly utilized as a reference for comparing the NLO properties of other materials. Notably, for hyperpolarizability (β) and polarizability (α), 1a.u. (atomic unit) = 0.008639×10^{-30} and 0.1482×10^{-24} e.s.u., respectively. The dipole moment (μ) and polarizability (α) of the titled compounds are presented in Table 7. The dipole moment directions relative to the input files' Cartesian axes are illustrated in Fig. 9. The dipole moment increases in the presence of nitro groups in compounds **3** and **4**, with the negative pole oriented toward the electron-withdrawing nitrobenzene. The polarizability (α) increases progressively in the order: **1**<**2**<**3**<**4**, as the amino and nitro groups contribute to the enhanced mobility of the electrons.

Table 8 shows the first static hyperpolarizability (β) and its components for compounds **1**–**4**, revealing a significant increase in β total compared to urea due to the presence of amino and nitro groups. The $\beta_{total}/\beta_{urea}$ ratios for compounds **1**–**4** are 2.7, 28, 25, and 50, respectively. This enhancement is linked to the nitro group's strong withdrawing and the amino group's donor effects. Specifically, compound **4**, with the highest ratio (50), exhibits charge transfer from the amino benzene to the nitro benzene *via* the pyridine ring. This result suggests that these compounds, particularly **4**, are promising for optoelectronics and other industrial applications.

Table 7 — Dipole moment (μ) and polarizability (α) of compounds 1–4 and urea

Compound	1	2	3	4	Urea
μ_x	0.0000	1.0444	–5.5934	–6.1136	0.0018
μ_y	0.0000	0.5602	3.8480	2.7337	–3.8594
μ_z	–1.9409	0.6556	–0.0376	–0.6278	0.0043
μ_{total} (Debye)	1.9409	1.3545	6.7895	6.7264	3.8594
α_{xx}	22.2670	48.8482	50.0167	53.4087	5.29068
α_{yx}	2.7113	–0.4928	0.7280	1.4807	–0.0001
α_{yy}	44.7111	37.1399	37.8360	40.8614	5.4525
α_{zx}	0.0000	2.3416	2.5806	2.7374	0.00849
α_{zy}	0.0000	0.2496	0.9433	0.7395	–0.0001
α_{zz}	35.0275	22.6754	23.4360	23.9333	3.26759
$<\alpha>$ (a.u.)	229.4560	244.4325	250.3378	265.8920	31.5163
$<\alpha>\times10^{-24}$(e.s.u.)	34.0054	36.2249	37.1001	39.4052	4.6707

Table 8 — First static hyperpolarizability (β) and their individual components for compounds 1–4 and urea

Compound	1	2	3	4	Urea
β_{xxx}	0.0000	–7.3567	8.8663	13.1727	0.0003
β_{xxy}	0.0000	3.5800	–3.2751	–0.1129	0.3427
β_{yxy}	0.0000	–1.8227	0.8238	5.3289	–0.0006
β_{yyy}	0.0000	1.6325	1.2996	3.6321	–0.6013
β_{xxz}	0.0270	0.4379	–0.3651	–0.8952	0.0004
β_{yxz}	0.1090	0.1467	0.0083	–0.1530	0.0559
β_{yyz}	–0.1534	–0.0992	0.1400	0.1834	0.0003
β_{zxz}	0.0000	0.0764	–0.4865	–0.5435	–0.0001
β_{zyz}	0.0000	0.0086	0.2086	0.2117	–0.1119
β_{zzz}	–0.8774	0.0589	0.0006	–0.0550	0.0001
β (a.u.)	116.1973	1215.5681	1085.0920	2124.9127	42.8800
$\beta_{total}\times10^{-30}$(e.s.u.)	1.0038	10.5013	9.3741	18.3571	0.3704
$\beta_{total}/\beta_{urea}$	2.7	28	25	50	1

Conclusions

In this study, we performed DFT calculations at the wB97XD/Def2TZVPP level for compounds **1**–**4** to investigate their electronic properties and thus assess their applicability in modern technology. The amino group's donating effect and the nitro group's withdrawing effect influence the electronic properties of the compounds. Detailed calculations were performed for global reactivity descriptors, Mulliken and NBO charges, MEP surfaces, NBO analysis, UV–Vis absorption characteristics, and NLO parameters. The HOMO and LUMO are concentrated on the amino and nitro benzene rings, respectively, indicating charge transfer from the amino to the nitro group, as observed in compound **4**. The energy gaps ($E_{LUMO} - E_{HOMO}$), ranging from 6.9470 to 8.8026 eV, suggest that compounds **1**–**4** are chemically stable, and compound **4** exhibits the smallest energy gap and highest softness. UV–Vis spectral analysis shows that the $\pi \rightarrow \pi^*$ transitions dominate, with the HOMO–LUMO transition wavelength increasing in the order of **4**>**3**>**2**>**1**. The hyperpolarizability (β) values exhibit significant variation, with $\beta_{total}/\beta_{urea}$ for compounds **1**, **2**, **3**, and **4** being 2.7, 28, 25 and 50, respectively. These promising results suggest potential applications of these compounds, especially compound **4**, in optoelectronics, technology, and industry.

Supplementary Information

Supplementary information is available in the website http://nopr.niscpr.res.in/handle/123456789/58776.

References

1 Seferoğlu Z, Ihmels H & Şahin E, *Dye Pigment*, 113 (2015) 465.

2 Pelosi A G, Zucolotto Cocca L H, Luis M G, Abegão, Sciuti L F, Sciuti L F, Piguel S, Boni L D & Mendonça C R, *Dye Pigment*, 198 (2022) 109972.

3 Xiao S, Liu Z, Zhao J, Pei M, Zhang G & He W, *RSC Adv*, 6 (2016) 27119.

4 Tomoda H, Hirano T, Saito S, Mutai T & Araki K, *Bull Chem Soc Jpn*, 72 (1999) 1327.

5 Cocca L H Z, Pelosi A G, Valverde J V P, Bescont J L, Breton-Patient C, Piguel S, Mendonça C R & Boni L D, *J Photochem Photobio A: Chem,* 440 (2023) 114675.

6 Biswal P, Samser S, Nayak P, Chandrasekhar V & Venkatasubbaiah K, *J Org Chem*, 86 (2021) 6744.

7 Mathew E, Harshitha K R, Sarojini B K & Joe I H, *J Mol Struc*, 1311 (2024) 138353.
8 Hadji D, Baroudi B & Bensafi T, *J Mol Model*, 30 (2024) 117.
9 Lakhera S, Devlal K & Rana M, *Phys Scr*, 98 (2023) 115519.
10 Sıdır İ, Sıdır Y G & Kayagil İ, *Spectrochim Acta Part A: Mol Biomol Spec*, 81 (2011) 339.
11 Boukabcha N, Benmohammed A, Belhachemi M H M, Goudjil M, Yahiaoui S, Megrouss Y, Djafri A, Khelloul N, Benyehlou Z D, Djafri A & Chouaih A, *J Mol Struc*, 1285 (2023) 135492.
12 Choudhary V, Bhatt A, Dash D & Sharma N, *J Comp Chem*, 40 (2019) 2354.
13 Akman F, *Opt Quantum Elec*, 56 (2024) 1444.
14 Badran A, Ibrahim M A, Mohamed N & Mostafa M A, *J Mol Struct*, 1320 (2025) 139632.
15 Kumar M K, Jeyakumari A P, Anbalagan, G, Shinde V & Sriram S, *J Mat Sci: Mat Elec*, 30 (2019) 11931.
16 Agwupuye J A, Louis H, Unimuke T O, David P, Ubana E I & Moshood Y L, *J Mol Liq*, 337 (2012) 116458.
17 Frisch M J, Trucks G W, Schlegel H B, Scuseria G E, Robb M A, Cheeseman J R, Scalmani G, Barone V, Petersson G A, Nakatsuji H & Li X, *Gaussian 16, Revision a. 03*, (Gaussian, Inc., Wallingford CT. Gaussian16, Revision A 03) 2016.
18 Dennington R, Keith T A & Millam J M, *Gauss View (Version 6.0). Shawnee*, (KS: Semichem Inc) 2016.